Nano Research 2018, 11(12): 6417–6427
https://doi.org/10.1007/s12274-018-2166-x
Research Article
ISSN 1998-0124
CN 11-5974/O4

Highly fluorescent, photostable, and biocompatible silicon theranostic nanoprobes against *Staphylococcus aureus* infections

Xia Zhai, Bin Song, Binbin Chu, Yuanyuan Su, Houyu Wang (✉), and Yao He (✉)

Laboratory of Nanoscale Biochemical Analysis, Institute of Functional Nano & Soft Materials (FUNSOM), and Collaborative Innovation Center of Suzhou Nano Science and Technology (NANO-CIC), Soochow University, Suzhou 215123, China

Received: 9 June 2018
Revised: 30 July 2018
Accepted: 1 August 2018

KEYWORDS
fluorescent silicon nanoparticles,
Gram-positive bacteria,
Staphylococcus aureus,
prolonged,
extended period

ABSTRACT

Human health is severely threatened by bacterial infections, which fuel urgent demand for the development of novel theranostic agents that are suitable for diagnosing and combating bacterial infections. To meet this goal, we synthesized a new kind of theranostic probes, made of vancomycin (Van)-modified fluorescent silicon nanoparticles (SiNPs-Van). The new probes feature good selectivity for Gram-positive bacterial infections, favorable fluorescence, strong resistance to photobleaching (e.g., 12% loss of fluorescence intensity during 40 min continuous laser excitation in the presence of *Staphylococcus aureus* (*S. aureus*)), and good biocompatibility (e.g., cell viability > 95% during 24 h treatment). Because of these benefits, the probes were effective at prolonged (i.e., 8-day) fluorescence tracking of *S. aureus* infections *in vivo*, thus providing a visible and accurate way to evaluate treatment efficacy. Moreover, the resultant SiNPs-Van with a minimum inhibitory concentration (MIC) of ca. 0.5 μg/mL exhibited high antibacterial efficiency of 92.5%, superior to that (76.5%) of free Van with higher MIC of ca. 1 μg/mL.

1 Introduction

Public health has been overwhelmed by bacterial infections [1–5]. A consensus has been reached that the lethality could be greatly decreased if bacterial infections could be effectively diagnosed and treated at an early stage. Numerous techniques, such as bacterial culture, polymerase chain reaction (PCR), and sequencing, have been utilized for the analysis of pathogens to date [6–8]. Although these techniques are workable, they are to some extent time-consuming (e.g., several hours to days for bacterial culture and detection), and often involve tedious procedures [6–8]. To address these issues, targeted optical imaging of bacteria based on fluorescent dyes, proteins, or inorganic nanomaterials (e.g., rhodamine-modified vancomycin, green fluorescent protein, gold nanoparticles, and carbon nanotubes) has been intensively explored for

Address correspondence to Houyu Wang, hywang@suda.edu.cn; Yao He, yaohe@suda.edu.cn

preclinical and clinical applications owing to their short duration of data acquisition, facile manipulations, and low cost [9–18]. At present, a promising concept, that is optical-imaging-guided treatment of bacterial infections, fuels urgent demand for the fabrication of novel multifunctional theranostic probes, which allow for simultaneous detection and treatment of early-stage bacterial infections *in vivo* [19–21]. Furthermore, for estimating the efficacy of antimicrobial therapy in real time in an accurate manner, extensive efforts are required for designing new tools capable of lengthy tracking the development of bacterial infections during the therapeutic process [19–21].

On the other hand, silicon, as an abundant, low-cost, and environmentally friendly resource, has played key roles in myriad fields since the last century. Accompanied with significant advancement of nanotechnology, functional silicon nanostructures have attracted intensive research attention, among which fluorescent silicon nanoparticles (SiNPs) are of particular interest due to their unique optical characteristics [22–24]. Recent years have witnessed giant achievements in the fabrication of SiNPs featuring strong and stable fluorescence. For example, recent studies have demonstrated that under the same UV irradiation, SiNPs could retain nearly unchanged fluorescence during 180 min UV treatment, which is in sharp contrast to rapid (~ 10 min) fluorescence quenching of organic dyes (e.g., FITC) [24]. By virtue of these optical merits, SiNPs have been used in optoelectronic devices (e.g., light-emitting diodes (LEDs) and photodetectors) [25]. On the other hand, small (diameter < 10 nm) SiNPs have been employed in a first-in-human clinical trial owing to their outstanding biocompatibility [26, 27]. These exciting achievements suggest that the biocompatible and fluorescent SiNPs are high-performance optical probes, holding great promise for various biological and biomedical applications [28–38].

Herein, we present a new kind of fluorescent-SiNP-based theranostic probes whose surface are modified with vancomycin (Van, a clinical antibiotic for specifically and effectively treating Gram-positive bacterial infections). Because of SiNPs and Van, the resultant probes are capable of actively targeted, noninvasive, and prolonged fluorescence imaging, as well as high-efficacy treatment of *Staphylococcus aureus* (*S. aureus*) infections. Typically, the probes with small size (diameter ~ 3 nm) and strong green fluorescence (e.g., quantum yield ~ 25%) could be suitable for real-time and prolonged (e.g., 8 days) tracking of *S. aureus* infections *in vivo*. In addition, the newly developed theranostic probes feature an antimicrobial effect with an antibacterial rate of ca. 92.5%, much better than that of free Van (ca. 76.5% antibacterial rate).

2 Experimental

2.1 Preparation of Van-modified fluorescent silicon nanoparticles (SiNPs-Van)

The amine-terminated fluorescent SiNPs (NH_2-SiNPs) were prepared by a previously reported protocol [39]. To obtain purified SiNPs, 1,8-naphthalimide was removed by centrifugation at 6,000 rpm for 15 min, and excess silicon precursor (3-aminopropyl)trimethoxysilane ($C_6H_{17}NO_3Si$, APTMS) was eliminated by dialysis (M_W cutoff (MWCO): 1,000, Spectra/Pro). Next, to prepare SiNPs-Van, 5 mg of vancomycin powder was mixed with 100 μL of N-(3-(dimethylamino)propyl)-N′-ethylcarbodiimide hydrochloride (EDC; 50 mg/mL) and 25 μL of N-hydroxysuccinimide (NHS; 50 mg/mL) at 4 ℃ with gentle shaking for 15 min in that order. After that, the activated vancomycin was further incubated with 50 μL of NH_2-SiNPs for 12 h at 4 ℃ with gentle shaking in the dark to synthesize SiNPs-Van. To remove the excess unreacted Van, the resulting mixture was transferred into Nanosep centrifugal devices (MWCO, 10 kDa; Millipore) and washed with phosphate buffered saline (PBS) several times with centrifugation at 7,500 rpm for 15 min. The final mixture was stored at 4 ℃ in the dark. The loading amounts of Van on SiNPs (0.617 mg Van per mg of SiNPs) could be calculated based on the calibration absorption curves of Van (Fig. S1 in the Electronic Supplementary Material (ESM)).

2.2 Bacterial culture

Gram-negative *Escherichia coli* (*E. coli*) and Gram-positive *S. aureus* were selected as experimental models in our study. Bacterial cells were grown in the Luria–Bertani

(LB) medium with shaking at 250 rpm and 37 ℃. After that, the bacterial cells were collected via centrifugation at 10,000 rpm and 4 ℃, then washed with PBS two times and resuspended in PBS. Prior to analysis, the collected bacterial suspensions were diluted with the culture medium to the desired concentrations, which were determined by counting colony-forming units (CFUs) or by measuring optical density (OD) of the medium at 600 nm (OD_{600}).

2.3 SEM characterization of the bacteria treated with SiNPs-Van

The morphological features of *E. coli* and *S. aureus* (5×10^9 CFU/mL) treated with SiNPs-Van (15.2 mg/mL) were directly examined using scanning electron microscopy (SEM). After 1.5 h treatment, the bacteria were harvested and processed for visualization, and then fixed with 4% paraformaldehyde (PFA) for 20 min at room temperature, followed by several dehydration steps in a series of ethanol solutions of different concentrations (e.g., 50%, 70%, 80%, 90%, 95%, and 100%, each for 10 min).

2.4 A bacterial imaging assay

Next, 20 μL of a bacterial suspension (5×10^9 CFU/mL) was treated with SiNPs-Van (15.2 mg/mL) for 1.5 h in a shaking incubator (200 rpm) at 37 ℃. Then, the bacterial cells were centrifuged at the speed of 8,000 rpm for 10 min and washed twice with PBS to remove excess SiNPs-Van. After that, 20 μL of the obtained solution was placed onto a microscope slide, covered with a coverslip, and then imaged under a confocal microscope (Leica, TCS-SP5). The region of interest (ROI) was analyzed by the software (Leica LAS AF Lite).

2.5 Prolonged imaging of *S. aureus* infection

To construct a mouse model of *S. aureus* infection, 50 μL of *S. aureus* (10^9 CFU/mL) was subcutaneously injected into the right caudal thigh. Accordingly, 50 μL of PBS was subcutaneously injected into the left caudal thigh to set up the control group. At 24 h after injection, the SiNPs-Van nanoprobes in the same amounts (7.86 mg/mL) were subcutaneously injected into the infected sites and control sites. An IVIS Lumina imaging system was employed to obtain fluorescence images. On the other hand, the mice injected only into the right caudal thigh were subcutaneously injected with SiNPs-Van (7.86 mg/mL). Fluorescent images were captured at scheduled time points (0 and 0.5 days, 1 day, 1.5, 2, 4, 6, and 8 days). Meanwhile, the mice treated at each time point were euthanized and the infected tissues were excised from the mice. After that, the tissues were homogenized in sterile PBS (according to the weight of tissues, 0.01 g/mL). The bacteria collected from the infected tissue dispersions were cultured on an agarose medium for 16 h, and corresponding numbers of colonies were obtained via the classic plate counting method.

2.6 The antibacterial effect of SiNPs-Van *in vivo*

At 24 h postinfection with *S. aureus*, the infected mice were injected with 75 μL of PBS, Van, or SiNPs-Van subcutaneously into infected sites three times every 24 h. The infected wounds of mice were imaged every 2 days. After 4-day treatment, the mice of each group (n = 3) were euthanized, and infected tissues were excised from mice; the tissues were homogenized in sterile PBS (according to the weight of tissues, 0.01 g/mL). Aliquots of diluted homogenized infected tissues were plated on agar, where the grown colonies were counted. The antibacterial rate was calculated based on the following formula: Antibacterial rate (%) = $(N_{control} - N_{experiment})/N_{control} \times 100\%$, where $N_{control}$ and $N_{experiment}$ stand for the numbers of bacterial colonies in PBS (control) and Van (or SiNPs-Van) (experiment) treated samples, respectively. The other mice were euthanized, and infected tissues were excised on the 8th day, fixed in a 4% formaldehyde solution for 24 h at room temperature, then embedded in paraffin, and cut into 5-μm-thick sections for hematoxylin and eosin (H&E) staining. H&E assays were performed according to the standard protocols.

2.7 Biocompatibility of SiNPs-Van

An 3-(4,5-dimethylthiazol-2-yl)-2,5-diphenyltetrazolium bromide (MTT) assay was used to evaluate *in vitro* cytotoxicity of SiNPs-Van. For the MTT assay, MDA-MB-231 and HREC cells were used as the representative cancer cells and normal cells. They were incubated with

SiNPs, SiNPs-Van, or Van at different concentrations in culture media for 24 h. The treated cells were then incubated with MTT (5 mg/mL) at 37 °C for 4 h, followed by cell lysis with acidified sodium dodecyl sulfate (SDS). The microplate reader (Bio-Rad 680, USA) was used to measure the absorbance of cell lysates at 570 nm. Next, to evaluate the biosafety of SiNPs-Van *in vivo*, the distribution of SiNPs-Van and the corresponding histological evaluation were carried out. First, the infected mice were injected with 75 μL of SiNPs-Van. Next, various organs of the mice including the heart, liver, spleen, lungs, and kidneys were excised at 6 h and 8 days postinjection. The organs were imaged using an IVIS Lumina imaging system, in which the measured fluorescence signals from these organs were employed to describe the biodistribution of SiNPs-Van. In addition, the main organs were also stained with H&E after 8-day treatment with SiNPs-Van.

2.8 Statistical analysis

Error bars represent standard deviation obtained from three independent measurements. All the statistical analyses were performed in the Origin software. The statistical significance of differences was determined by one-way ANOVA. $P < 0.05$ (*), $p < 0.01$ (**), and $p < 0.001$ (***) were used to indicate statistical difference.

3 Results and discussion

3.1 Preparation and characterization of SiNPs-Van

As schematically illustrated in Fig. 1(a), fluorescent SiNPs were first synthesized based on a previously reported method [39]. Related transmission electron microscopy (TEM), UV, and photoluminescence (PL) procedures for characterization of SiNPs are provided in Fig. S2 (in the ESM). The surface of the as-prepared SiNPs is terminated with amino groups ($-NH_2$), which can be covalently coupled with carboxyl groups (–COOH) of Van molecules by EDC coupling chemistry [35, 39–41]. The loading amounts of Van on SiNPs (0.617 mg Van per milligram of SiNPs) could be calculated based on the calibration absorption curves of Van (Fig. S1 in the ESM). Figure 1(b) describes

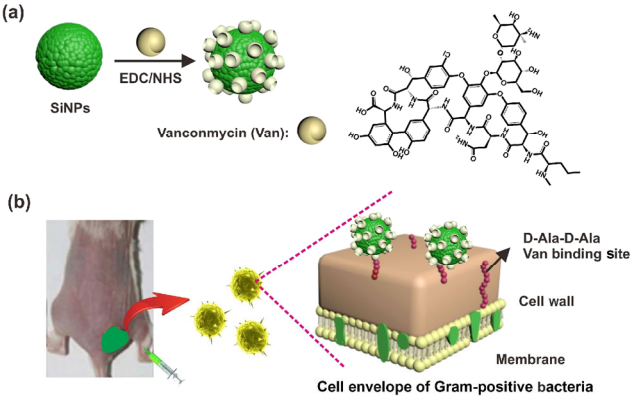

Figure 1 The synthetic route of SiNPs-Van (a) and the corresponding Gram-positive bacteria-targeted imaging and therapeutic mechanism (b).

the mechanism for specifically monitoring and killing Gram-positive bacteria *in vivo* by SiNPs-Van. As previously reported, there exists a strong binding affinity between Van and Gram-positive bacteria ascribed to the formation of five-hydrogen bond networks between the heptapeptide skeleton of Van and the D-alanyl (Ala)-D-Ala moiety in the cell wall of Gram-positive bacteria [40–42]. Therefore, the resultant SiNPs-Van can selectively distinguish Gram-positive bacteria due to the strong affinity of Van for Gram-positive bacteria. Due to the high surface-to-volume ratio of nanoparticles, abundant Van ligands can be linked to SiNP surface, enhancing the interaction between probes and bacteria [28, 40, 43]. By virtue of their strong and stable fluorescence as well as high antibacterial efficiency, such SiNPs-Van probes enabled prolonged and noninvasive tracking of Gram-positive bacterial infections, and moreover, displayed superior antibacterial efficiency compared to free Van.

Figure 2(a) presents the TEM and high-resolution TEM (HRTEM) images of resultant fluorescent SiNPs-Van, which appear as spherical particles. Figure 2(b) displays the size distribution of SiNPs-Van, calculated by measuring 200 particles in a TEM image. The average size of SiNPs-Van was ~ 2.8 nm, slightly larger than that (~ 2.5 nm) of pure SiNPs (Fig. S3 in the ESM). Dynamic light scattering (DLS) measurement of the SiNPs-Van in an aqueous solution was also performed (Fig. 2(c)), revealing that pure SiNPs had a DLS diameter of ~ 3.8 nm, relatively smaller than that (~ 5.8 nm) of SiNPs-Van. These data indicate successful

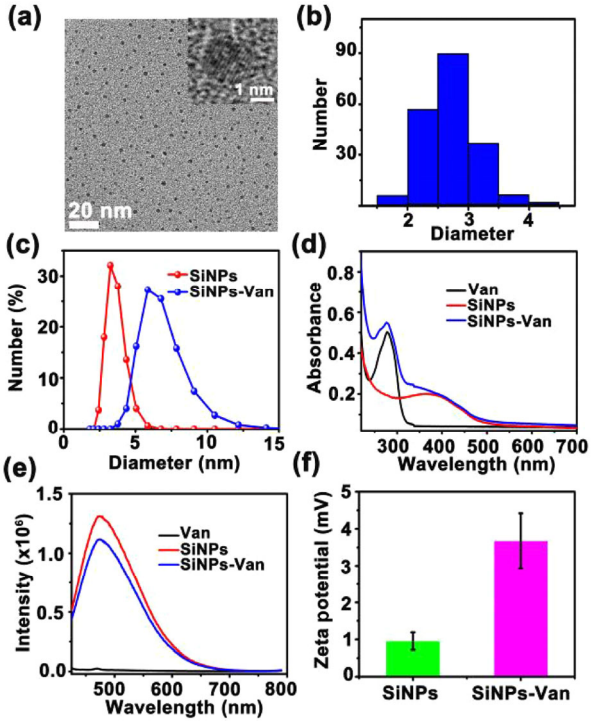

Figure 2 Characterization procedures for the as-prepared SiNPs-Van. (a) TEM and HRTEM (inset) images of SiNPs-Van. (b) Size distribution of SiNPs-Van. (c) DLS spectra of SiNPs (red curve) and SiNPs-Van (blue curve). (d) UV absorbance and (e) PL spectra of Van (black curve), SiNPs (red curve), and SiNPs-Van (blue curve) (λ_{ex} = 405 nm). (f) Zeta potential of SiNPs and SiNPs-Van.

loading of Van onto the SiNPs [44]. The modification by Van was next confirmed by UV–vis absorbance spectra and Zeta potential. As depicted in Fig. 2(d), the SiNPs-Van show two typical peaks at 280 and 380 nm, which were assigned to Van and SiNPs, respectively [39, 42, 45]. The PL spectrum of SiNPs-Van was similar to that of pure SiNPs, as revealed in Fig. 2(e). During excitation at 405 nm, both SiNPs-Van and SiNPs displayed the characteristic emission peak at 480 nm. As for Zeta potential, when Van was linked to the SiNP surface, Zeta potential climbed from 0.93 to 3.7 mV (Fig. 2(f)). Besides, no significant fluorescence quenching was observed for the as-prepared SiNPs-Van during 35-day storage in PBS (Fig. S4 in the ESM).

3.2 Distinguishing Gram-positive and Gram-negative bacteria

To validate the feasibility of selective recognition of Gram-positive bacteria by SiNPs-Van, *in vitro* bacterial imaging of SiNPs-Van for various bacteria was performed. The bacterial suspension was treated with SiNPs-Van (Fig. S5 in the ESM) and imaged by means of a confocal microscope. Figure 3(a) shows that distinct green fluorescence was observed in the presence of Gram-positive *S. aureus* bacteria, whereas no significant fluorescence was detected in the group of Gram-negative *E. coli* bacteria, suggesting that SiNPs-Van were able to selectively stain Gram-positive bacteria. In comparison, pure-SiNP-treated bacteria (control group) displayed weak fluorescence with *S. aureus* and *E. coli*. Additionally, SiNPs-Van probes could discriminate *S. aureus* from *E. coli* in the mixture group containing two species of bacterial cells (Fig. S6 in the ESM). The selectivity of SiNPs-Van for Gram-positive bacteria was next confirmed by SEM data. As shown in Fig. 3(b), the rough and wrinkled cell wall of bacteria was observed only in the SiNPs-Van-treated *S. aureus* group, whereas the smooth cell wall

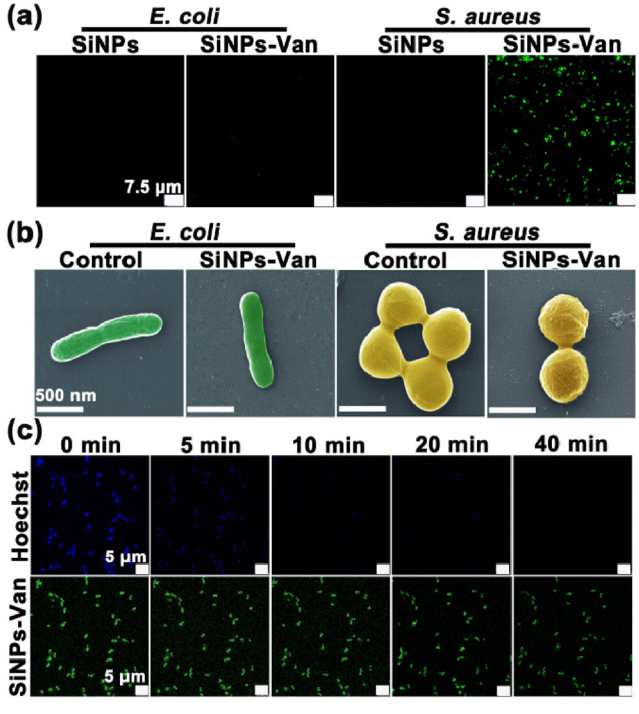

Figure 3 Selectivity of SiNPs-Van for Gram-positive bacteria. (a) Confocal fluorescence images and (b) SEM images of *E. coli* and *S. aureus* incubated with SiNPs or SiNPs-Van. (c) Confocal fluorescence images of *S. aureus* stained with Hoechst or SiNPs-Van under the continual excitation for 40 min. The final concentration of SiNPs-Van nanoprobes in the mixtures was 7.6 mg/mL (4.7 mg/mL SiNPs and 2.9 mg/mL Van) and the final concentration of SiNPs was 4.7 mg/mL.

was seen in other (control) groups, suggesting that the surface of *S. aureus* bacteria was abundantly surrounded by SiNPs-Van; this finding is well consistent with the above-mentioned confocal imaging data. Notably, green fluorescence signals from SiNPs-Van were stable and bright (e.g., intensity decreased by 12% under 40 min continual laser irradiation) due to excellent photostability of SiNPs [32–39]. In comparison, the blue fluorescence signals of Hoechst, a conventional fluorescent organic dye, rapidly vanished after 5 min continuous irradiation (e.g., an 80% decrease in intensity; Fig. 3(c)). These data indicated that this kind of SiNP-based photostable probes is suitable for prolonged imaging of bacteria.

3.3 Prolonged tracking of *S. aureus* infections *in vivo*

Taking advantage of their excellent selectivity, strong photostability, and good sensitivity, we next employed the newly developed SiNPs-Van probes for prolonged *in vivo* tracking of *S. aureus* infections. To construct a mouse model of *S. aureus* infection, 50 μL of (10^9 CFU/mL) *S. aureus* was subcutaneously injected into the right caudal thigh. As a control, the left caudal thigh of the mice was injected with PBS. The SiNPs-Van nanoprobes in the same amount (7.86 mg/mL) were then subcutaneously injected into both the infected site and control site. As revealed in Fig. 4(a), the distinct and stable signal of probes became detectable up to 24 h in the infected site, while the signal of probes quickly disappeared in the control site within 9 h. Additionally, as shown in the corresponding time-dependent fluorescence intensity profiles from two sites (Fig. 4(b)), the fluorescence intensities in the infected sites changed only a little (dropped by 23% at 24 h postinjection), whereas the intensities in the control sites declined rapidly (a 34.5% decrease in intensity at 9 h postinjection) and the fluorescent signal was hardly observed at 24 h postinjection. Of particular significance, by virtue of good photostability and specificity of SiNPs-Van, the developed probes had the ability to image *S. aureus* infections *in vivo* for an extended period (up to 8 days), suggesting lengthy retention of SiNPs-Van in the infected sites. As displayed in Fig. 4(c), the fluorescence signals greatly decayed by the 8th day, probably because of the enhanced therapeutic

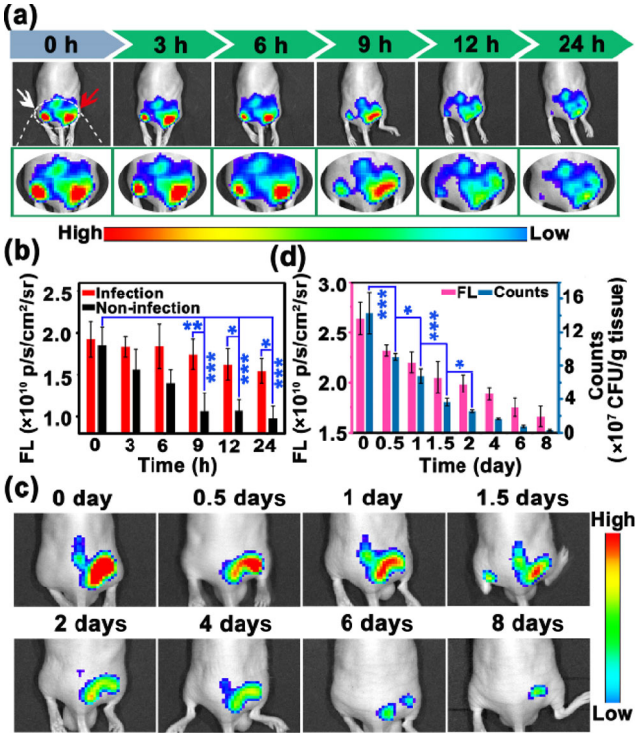

Figure 4 Long-term tracking of *S. aureus* infection *in vivo*. (a) *In vivo* imaging of infected sites (right, as the red arrow indicates) and uninfected sites (left, as the white arrow indicates) treated with SiNPs-Van in same amounts (7.86 mg/mL, 50 μL) at various time points and (b) corresponding time-dependent FL intensity profiles of infected sites and uninfected sites (* $p < 0.05$, ** $p < 0.01$ and *** $p < 0.001$). (c) Long-term *in vivo* imaging of *S. aureus*-infected mice 8 days after SiNPs-Van injection (7.86 mg/mL, 50 μL) and (d) corresponding time-dependent FL intensities and numbers of *S. aureus* colonies (counts) at infected sites. The bacteria collected from the infected tissue dispersions were cultured on an agarose medium for 16 h, and the corresponding numbers of colonies were obtained via the classic plate counting method. Excitation wavelength: 460 nm; emission wavelength: 520 nm.

effect of SiNPs-Van. The relation between fluorescence intensities and numbers of *S. aureus* cells in the infected sites is revealed in Fig. 4(d). Specifically, the fluorescent signal intensities declined along with the decrease in cell numbers at the infected sites. On the contrary, for the previously reported bacteria-targeted fluorescent probes (e.g., a deep-red fluorescent squaraine rotaxane scaffold with two appended bis(zinc(II)-dipicolylamine) (bis(Zn-DPA))), fluorescence quickly disappeared at the infected site within 21 h [46]. The SiNP-assisted real-time tracking of *S. aureus* infections in tissues by SiNPs-Van provided a visible and accurate way to evaluate the efficacy of antimicrobial

therapy for an extended period.

3.4 The antibacterial test of SiNPs-Van *in vitro* and *in vivo*

The antibacterial activity of SiNPs-Van *in vitro* was tested in the agar plate experiments (Fig. 5(a)) and liquid-medium turbidity assays (Figs. 5(b) and 5(c); for more details: see Refs. [47, 48]). As shown in Fig. 5(a), nearly no bacterial colonies were found in the group treated with SiNPs-Van for 7 h, indicating excellent antibacterial efficacy of SiNPs-Van *in vitro*. In contrast, compared to the control group, a 65% decrease in the number of bacterial colonies could be observed in free-Van-treated group under the same conditions, implying incomplete antibacterial efficacy of free Van against *S. aureus*. In addition, there was no significant difference in the numbers of bacterial colonies between the SiNP-treated group and control group, suggesting that pure SiNPs could not inhibit the growth of *S. aureus*. On the other hand, as shown in the turbidity of a bacterial suspension in Fig. 5(b), the LB liquid medium treated with SiNPs-Van was pellucid after 7 h incubation, whereas the medium without treatments and the medium treated with Van

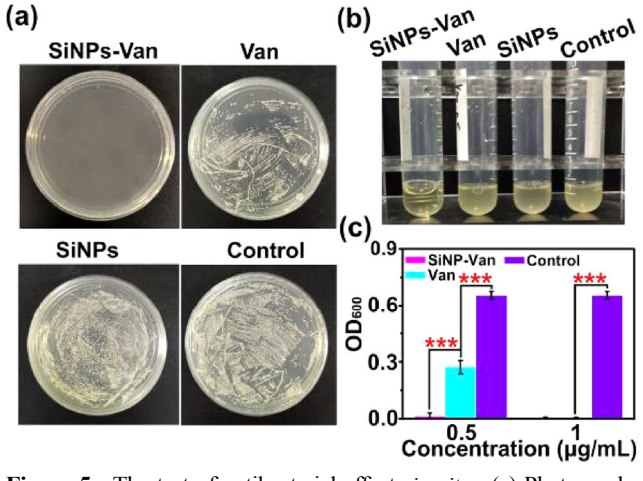

Figure 5 The test of antibacterial effects *in vitro*. (a) Photographs of the agar plates of *S. aureus* treated with SiNPs-Van at 1.31 μg/mL, Van at 0.5 μg/mL, or SiNPs at 0.81 μg/mL for 7 h. The agar plate of *S. aureus* without any treatment was set up as the control group. (b) The turbidity of bacterial suspensions treated with SiNPs-Van at 1.31 μg/mL, Van at 0.5 μg/mL, or SiNPs at 0.81 μg/mL for 7 h. The bacterial suspension without any treatment was set up as the control group. (c) OD_{600} values of bacterial suspensions treated with free Van or SiNPs-Van at various concentrations (*** $p < 0.001$).

or SiNPs for 7 h become turbid because of the rapid growth of *S. aureus*. For further quantitative evaluation, OD_{600} values of bacterial suspensions treated with free Van or SiNPs-Van at various concentrations were measured, and the values of OD_{600} against concentrations are plotted in Fig. 5(c). The corresponding minimum inhibitory concentration (MIC) of SiNPs-Van was 1.31 μg/mL (0.5 μg/mL Van), whereas the MIC of Van was 1 μg/mL. Moreover, the antibacterial rate of the newly developed SiNPs-Van probes stayed at greater than 90% during 8-day storage in PBS (Fig. S7 in the ESM).

To further evaluate the antibacterial effect of SiNPs-Van *in vivo*, *S. aureus*-infected mice were subdivided into three groups: injected with 75 μL of PBS, Van, or SiNPs-Van every 24 h three times, respectively. Corresponding photographs of the mice treated within 8 days are exhibited in Fig. 6(a). Typically, obvious ulceration and infected wounds were still observed on the 8th day in the PBS-treated group. In stark contrast, wound healing and scarring happened earlier and were faster in Van- and SiNPs-Van-treated groups. Additionally, as shown in histological images of infected skin tissues stained with H&E (Fig. 6(b)), hair follicles and blood vessels could be observed in SiNPs-Van- and free-Van-treated groups, manifesting the normal morphology of wound healing. In contrast, a significant number of extravasating neutrophils was observed in the PBS-treated group, pointing to the disrupted morphology in infected wounds. Besides, bacteria collected from the infected sites after 4-day treatment were counted by the bacterial culture method to further evaluate the efficacy of antimicrobial therapy *in vivo*. As displayed in Fig. 6(c), compared with the numerous bacterial colonies in the PBS-treated group, much fewer bacterial colonies were observed in the Van-treated group and almost no bacterial colonies were found in the SiNPs-Van group, indicating the superior antimicrobial activity of SiNPs-Van. Quantitatively, the antibacterial rate of SiNPs-Van was calculated and found to be 92.5%, greater than that (76.5%) of free Van. The SiNPs-Van tended to accumulate at the infected sites, and in this case, the local concentration of Van on the bacterial surface was higher than that with free Van owing to

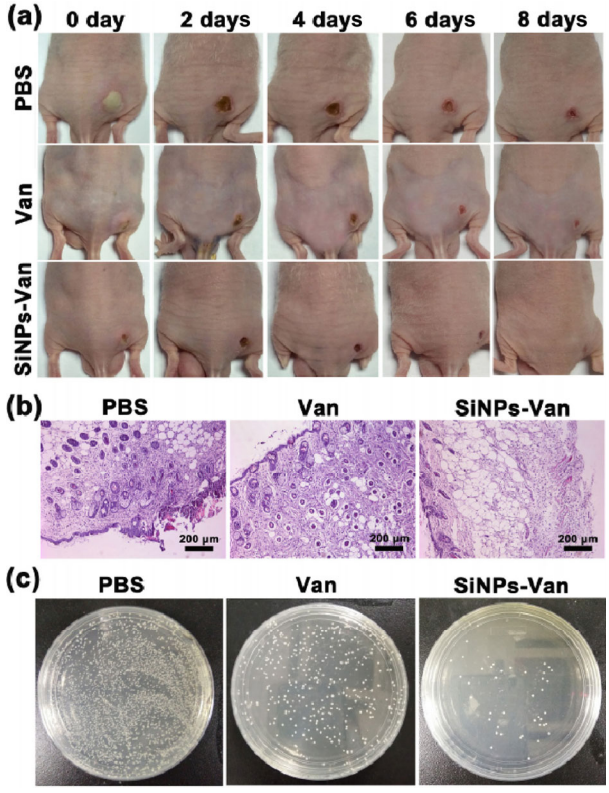

Figure 6 The *in vivo* antibacterial test of SiNPs-Van. (a) Representative photographs of the *S. aureus* (5×10^7 CFU)-infected mice at 8 days postinjection in three treatment groups (PBS, Van, and SiNPs-Van). (b) Corresponding histological images of the infected skin tissues of mice in the three treatment groups. (c) Corresponding photographs of bacterial cultures from the skin tissues of infected mice in three treatment groups.

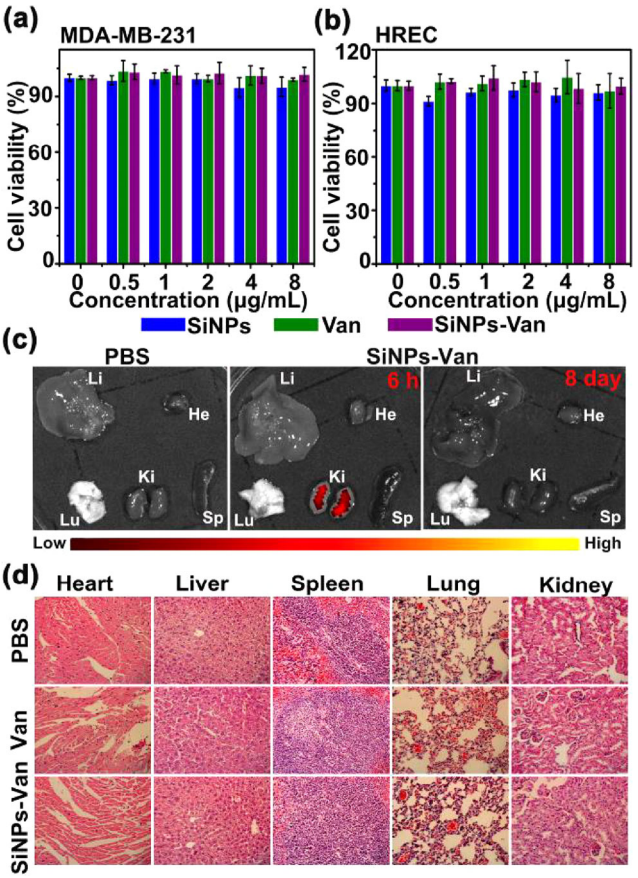

Figure 7 Biosafety assessment of SiNPs-Van *in vitro* and *in vivo*. Viability rates of MDA-MB-231 (a) and HREC cells (b) treated with different doses of PBS, vancomycin, or SiNPs-Van. (c) Biodistribution of SiNPs-Van in various organs including the heart (He), liver (Li), spleen (Sp), lungs (Lu), and kidneys (Ki) at 6 h and 8 days postinjection. The mice treated with PBS under the same conditions served as the control group. (d) Histological evaluation of different organs (the heart, liver, spleen, lungs, and kidneys) from mice treated with PBS, vancomycin, or SiNPs-Van.

the multivalence effect of nanocarriers, thus producing superior antibacterial activity [28, 40, 43].

3.5 *In vitro* and *in vivo* safety tests

The MTT assay was conducted to evaluate *in vitro* cytotoxicity of SiNPs-Van. As indicated in Figs. 7(a) and 7(b), the viability of MDA-MB-231 and HREC cells treated with SiNPs-Van at different concentrations for 24 h remained above 95%, indicating negligible cytotoxicity of SiNPs-Van. Ultimately, we also investigated the biocompatibility of SiNPs-Van *in vivo*. Next, the biodistribution of SiNPs-Van was evaluated. As indicated in Fig. 7(c), besides high accumulation at the infected sites, bright fluorescence was observed in kidneys, while no fluorescence was seen in other organs at 6 h postinjection; the fluorescence in kidneys was undetectable at 8 days postinjection, indicating that SiNPs-Van were efficiently eliminated from the mice through renal clearance owing to the small size of SiNPs-Van (~ 2.8 nm) [32]. The main organs resected from SiNPs-Van-treated (7.86 mg/mL) mice, including the heart, liver, spleen, lungs, and kidneys, were stained with H&E. As presented in Fig. 7(d), normal morphological features were observed in biopsy sections of all organs, indicating only weak toxicity of SiNPs-Van *in vivo*.

4 Conclusions

In summary, a new kind of high-performance theranostic probes made of Van-modified SiNPs (SiNPs-Van) was developed for prolonged imaging and

efficient therapy of *S. aureus* infections. Based on several desirable characteristics including distinct fluorescence parameters, good photostability, biocompatibility, and high selectivity for Gram-positive bacteria, the resultant SiNPs-Van enable prolonged tracking (8 days) and high-efficacy treatment (ca. 92.5% antibacterial rate) of *S. aureus* infections *in vivo*. Of note, if SiNPs-Van enter clinical practice in the future, this treatment may not be suitable for lactating mothers because some beneficial Gram-positive bacteria (e.g., *Lactobacillus reuteri*) might be killed as well. It is worthwhile to mention that there still exist major challenges for detecting the infection in deep tissues using the SiNPs-Van probes because of the short excitation and emission wavelengths of SiNPs. Therefore, future studies should focus on the development of near-infrared-light-emitting SiNP-based probes for improving the penetration depth of tissues *in vivo*; this task might be accomplished by doping SiNPs with phosphorus (P) or coupling SiNPs with erbium (Er) [49–51].

Acknowledgements

We appreciate financial support from the National Natural Science Foundation of China (Nos. 61361160412, 31400860, 21575096, and 21605109), Natural Science Foundation of Jiangsu Province of China (No. BK20170061) and a project funded by the Priority Academic Program Development of Jiangsu Higher Education Institutions (PAPD), 111 Project as well as Collaborative Innovation Center of Suzhou Nano Science and Technology (NANO-CIC).

Electronic Supplementary Material: Supplementary material (methods regarding preparation of SiNPs, data regarding characterizations of the 1,8-naphthalimide, APTMS and their mixed solution, quantification of vancomycin, the TEM image of pure SiNPs, the fluorescence stability test of SiNPs-Van, optimization of SiNPs-Van in the detection of Gram-positive bacteria, CLSM measurement of the mixture of *S. aureus* and *E. coli* treated by SiNPs-Van, and the antibacterial stability test of SiNPs-Van) is available in the online version of this article at https://doi.org/10.1007/s12274-018-2166-x.

References

[1] Blair, J. M. A.; Webber, M. A.; Baylay, A. J.; Ogbolu, D. O.; Piddock, L. J. V. Molecular mechanisms of antibiotic resistance. *Nat. Rev. Microbiol.* **2015**, *13*, 42–51.

[2] Hu, C. M. J.; Fang, R. H.; Wang, K. C.; Luk, B. T.; Thamphiwatana, S.; Dehaini, D.; Nguyen, P.; Angsantikul, P.; Wen, C. H.; Kroll, A. V.; Carpenter, C.; Ramesh, M.; Qu, V.; Patel, S. H.; Zhu, J.; Shi, W.; Hofman, F. M.; Chen, T. C.; Gao, W. W.; Zhang, K.; Chien. S.; Zhang, L. F. Nanoparticle biointerfacing by platelet membrane cloaking. *Nature* **2015**, *526*, 118–121.

[3] Brecher, M. E.; Hay, S. N. Bacterial contamination of blood components. *Clin. Microbiol. Rev.* **2005**, *18*, 195–204.

[4] Trampuz, A.; Zimmerli, W. Diagnosis and treatment of infections associated with fracture-fixation devices. *Injury* **2006**, *37*, S59–S66.

[5] Levy, S. B.; Marshall, B. Antibacterial resistance worldwide: Causes, challenges and responses. *Nat. Med.* **2004**, *10*, S122–S129.

[6] Ottesen, E. A.; Hong, J. W.; Quake, S. R.; Leadbetter, J. R. Microfluidic digital PCR enables multigene analysis of individual environmental bacteria. *Science* **2006**, *314*, 1464–1467.

[7] Kang, D. K.; Ali, M. M.; Zhang, K. X.; Huang, S. S.; Peterson, E.; Digman, M. A.; Gratton, E.; Zhao, W. A. Rapid detection of single bacteria in unprocessed blood using integrated comprehensive droplet digital detection. *Nat. Commun.* **2014**, *5*, 5427.

[8] Yuan, H. X.; Liu, Z.; Liu, L. B.; Lv, F. T.; Wang, Y. L.; Wang, S. Cationic conjugated polymers for discrimination of microbial pathogens. *Adv. Mater.* **2014**, *26*, 4333–4338.

[9] Yu, M. Q.; Wang, H.; Fu, F.; Li, L. Y.; Li, J.; Li, G.; Song, Y.; Swihart, M. T.; Song, E. Q. Dual-recognition förster resonance energy transfer based platform for one-step sensitive detection of pathogenic bacteria using fluorescent vancomycin-gold nanoclusters and aptamer-gold nanoparticles. *Anal. Chem.* **2017**, *89*, 4085–4090.

[10] Lai, H. Z.; Wang, S. G.; Wu, C. Y.; Chen, Y. C. Detection of *Staphylococcus aureus* by functional gold nanoparticle-based affinity surface-assisted laser desorption/ionization mass spectrometry. *Anal. Chem.* **2015**, *87*, 2114–2120.

[11] Cheng, D.; Yu, M. Q.; Fu, F.; Han, W. Y.; Li, G.; Xie, J. P.; Song, Y.; Swihart, M. T.; Song, E. Q. Dual recognition strategy for specific and sensitive detection of bacteria using aptamer-coated magnetic beads and antibiotic-capped gold nanoclusters. *Anal. Chem.* **2016**, *88*, 820–825.

[12] Hernandez, F. J.; Huang, L. Y.; Olson, M. E.; Powers, K. M.; Hernandez, L. I.; Meyerholz, D. K.; Thedens, D. R.; Behlke, M. A.; Horswill, A. R.; McNamara II, J. O.

Noninvasive imaging of *Staphylococcus aureus* infections with a nuclease-activated probe. *Nat. Med.* **2014**, *20*, 301–306.

[13] Setyawati, M. I.; Kutty, R. V.; Tay, C. Y.; Yuan, X.; Xie, J. P.; Leong, D. T. Novel theranostic DNA nanoscaffolds for the simultaneous detection and killing of *Escherichia coli* and *Staphylococcus aureus*. *ACS Appl. Mater. Interfaces* **2014**, *6*, 21822–21831.

[14] Tang, Q.; Liu, J.; Shrestha, L. K.; Ariga, K.; Ji, Q. M. Antibacterial effect of silver-incorporated flake-shell nanoparticles under dual-modality. *ACS Appl. Mater. Interfaces* **2016**, *8*, 18922–18929.

[15] Zheng, K. Y.; Setyawati, M. I.; Leong, D. T.; Xie, J. P. Antimicrobial gold nanoclusters. *ACS Nano* **2017**, *11*, 6904–6910.

[16] Zheng, K. Y.; Setyawati, M. I.; Lim, T. P.; Leong, D. T.; Xie, J. P. Antimicrobial cluster bombs: Silver nanoclusters packed with daptomycin. *ACS Nano* **2016**, *10*, 7934–7942.

[17] Zheng, K. Y.; Setyawati, M. I.; Leong, D. T.; Xie, J. P. Antimicrobial silver nanomaterials. *Coord. Chem. Rev.* **2018**, *357*, 1–17.

[18] Ariga, K.; Mori, T.; Li, J. B. Langmuir nanoarchitectonics from basic to frontier. *Langmuir*, in press, DOI: 10.1021/acs.langmuir.8b01434.

[19] Ferreira, K.; Hu, H. Y.; Fetz, V.; Prochnow, H.; Rais, B.; Müller, P. P.; Brönstrup, M. Multivalent siderophore-DOTAM conjugates as theranostics for imaging and treatment of bacterial infections. *Angew. Chem., Int. Ed.* **2017**, *56*, 8272–8276.

[20] Zhao, Z. W.; Yan, R.; Yi, X.; Li, J. L.; Rao, J. M.; Guo, Z. Q.; Yang, Y. M.; Li, W. F.; Li, Y. Q.; Chen, C. Y. Bacteria-activated theranostic nanoprobes against methicillin-resistant *Staphylococcus aureus* infection. *ACS Nano* **2017**, *11*, 4428–4438.

[21] Chen, X. S.; Wo, F. J.; Jin, Y.; Tan, J.; Lai, Y.; Wu, J. M. Drug-porous silicon dual luminescent system for monitoring and inhibition of wound infection. *ACS Nano* **2017**, *11*, 7938–7949.

[22] Dasog, M.; Kehrle, J.; Rieger, B.; Veinot, J. G. C. Silicon nanocrystals and silicon-polymer hybrids: Synthesis, surface engineering, and applications. *Angew. Chem., Int. Ed.* **2016**, *55*, 2322–2339.

[23] Su, Y. Y.; Ji, X. Y.; He, Y. Water-dispersible fluorescent silicon nanoparticles and their optical applications. *Adv. Mater.* **2016**, *28*, 10567–10574.

[24] Peng, F.; Su, Y. Y.; Zhong, Y. L.; Fan, C. H.; Lee, S. T.; He, Y. Silicon nanomaterials platform for bioimaging, biosensing, and cancer therapy. *Acc. Chem. Res.* **2014**, *47*, 612–623.

[25] Yang, L.; Liu, Y.; Zhong, Y. L.; Jiang, X. X.; Song, B.; Ji, X. Y.; Su, Y. Y.; Liao, L. S.; He, Y. Fluorescent silicon nanoparticles utilized as stable color converters for white light-emitting diodes. *Appl. Phys. Lett.* **2015**, *106*, 173109.

[26] Park, J. H.; Gu, L.; von Maltzahn, G.; Ruoslahti, E.; Bhatia, S. N.; Sailor, M. J. Biodegradable luminescent porous silicon nanoparticles for *in vivo* applications. *Nat. Mater.* **2009**, *8*, 331–336.

[27] Phillips, E.; Penate-Medina, O.; Zanzonico, P. B.; Carvajal, R. D.; Mohan, P.; Ye. Y. P.; Humm, J.; Gönen, M.; Kalaigian, H.; Schöder, H.; Strauss, H. W.; Larson, S. M.; Wiesner, U.; Bradbury, M. S. Clinical translation of an ultrasmall inorganic optical-PET imaging nanoparticle probe. *Sci. Transl. Med.* **2014**, *6*, 260ra149.

[28] Zhang, X. D.; Chen, X. K.; Yang, J. J.; Jia, H. R.; Li, Y. H.; Chen, Z.; Wu, F. G. Quaternized silicon nanoparticles with polarity-sensitive fluorescence for selectively imaging and killing Gram-positive bacteria. *Adv. Funct. Mater.* **2016**, *26*, 5958–5970.

[29] Ariga, K.; Leong, D. T.; Mori, T. Nanoarchitectonics for hybrid and related materials for Bio-oriented applications. *Adv. Funct. Mater.* **2018**, *28*, 1702905.

[30] Tay, C. Y.; Setyawati, M. I.; Xie, J. P.; Parak, W. J.; Leong, D. T. Back to basics: Exploiting the innate physic-chemical characteristics of nanomaterials for biomedical applications. *Adv. Funct. Mater.* **2014**, *24*, 5936–5955.

[31] Komiyama, M.; Mori, T.; Ariga, K. Molecular imprinting: Materials nanoarchitectonics with molecular information. *Bull. Chem. Soc. Jpn.* **2018**, *91*, 1075–1111.

[32] Ji, X. Y.; Peng, F.; Zhong, Y. L.; Su, Y. Y.; Jiang, X. X.; Song, C. X.; Yang, L.; Chu, B. B.; Lee, S. T.; He, Y. Highly fluorescent, photostable, and ultrasmall silicon drug nanocarriers for long-term tumor cell tracking and *in-vivo* cancer therapy. *Adv. Mater.* **2015**, *27*, 1029–1034.

[33] Wu, S. C.; Zhong, Y. L.; Zhou, Y. F.; Song, B.; Chu, B. B.; Ji, X. Y.; Wu, Y. Y.; Su, Y. Y.; He, Y. Biomimetic preparation and dual-color bioimaging of fluorescent silicon nanoparticles. *J. Am. Chem. Soc.* **2015**, *137*, 14726–14732.

[34] Pang, J. Y.; Su, Y. Y.; Zhong, Y. L.; Peng, F.; Song, B.; He, Y. Fluorescent silicon nanoparticle-based gene carriers featuring strong photostability and feeble cytotoxicity. *Nano Res.* **2016**, *9*, 3027–3037.

[35] Song, C. X.; Zhong, Y. L.; Jiang, X. X.; Peng, F.; Lu, Y. M.; Ji, X. Y.; Su, Y. Y.; He, Y. Peptide-conjugated fluorescent silicon nanoparticles enabling simultaneous tracking and specific destruction of cancer cells. *Anal. Chem.* **2015**, *87*, 6718–6723.

[36] Chu, B. B.; Wang, H. Y.; Song, B.; Peng, F.; Su, Y. Y.; He, Y. Fluorescent and photostable silicon nanoparticles sensors for real-time and long-term intracellular pH measurement in live cells. *Anal. Chem.* **2016**, *88*, 9235–9242.

[37] Chu, B. B.; Song, B.; Ji, X. Y.; Su, Y. Y.; Wang, H. Y.; He, Y. Fluorescent silicon nanorods-based ratiometric sensors for long-term and real-time measurements of intracellular pH in live cells. *Anal*. *Chem*. **2017**, *89*, 12152–12159.

[38] Ji, X. Y.; Guo, D. X.; Song, B.; Wu, S. C.; Chu, B. B.; Su, Y. Y.; He, Y. Traditional Chinese medicine molecule-assisted chemicalsynthesis of fluorescent anti-cancer silicon nanoparticles. *Nano Res*., in press, DOI: 10.1007/s12274-018-1976-1.

[39] Zhong, Y. L.; Sun, X. T.; Wang, S. Y.; Peng, F.; Bao, F.; Su, Y. Y.; Li, Y. Y.; Lee, S. T.; He, Y. Facile, large-quantity synthesis of stable, tunable-color silicon nanoparticles and their application for long-term cellular imaging. *ACS Nano* **2015**, *9*, 5958–5967.

[40] Kell, A. J.; Stewart, G.; Ryan, S.; Peytavi, R.; Boissinot, M.; Huletsky, A.; Bergeron, M. G.; Simard, B. Vancomycin-modified nanoparticles for efficient targeting and preconcentration of Gram-positive and Gram-negative bacteria. *ACS Nano* **2008**, *2*, 1777–1788.

[41] Qi, G. B.; Li, L. L.; Yu, F. Q.; Wang, H. Vancomycin-modified mesoporous silica nanoparticles for selective recognition and killing of pathogenic Gram-positive bacteria over macrophage-like cells. *ACS Appl*. *Mater*. *Interfaces* **2013**, *5*, 10874–10881.

[42] Choi, S. K.; Myc, A.; Silpe, J. E.; Sumit, M.; Wong, P. T.; McCarthy, K.; Desai, A. M.; Thomas, T. P.; Kotlyar, A.; Holl, M. M. B.; Orr, B. G.; Baker, J. R. Dendrimer-based multivalent vancomycin nanoplatform for targeting the drug-resistant bacterial surface. *ACS Nano* **2013**, *7*, 214–228.

[43] Li, X. N.; Robinson, S. M.; Gupta, A.; Saha, K.; Jiang, Z. W.; Moyano, D. F.; Sahar, A.; Riley, M. A.; Rotello, V. M. Functional gold nanoparticles as potent antimicrobial agents against multi-drug-resistant bacteria. *ACS Nano* **2014**, *8*, 10682–10686.

[44] Jiang, A. R.; Song, B.; Ji, X. Y.; Peng, F.; Wang, H. Y.; Su, Y. Y.; He, Y. Doxorubicin-loaded silicon nanoparticles impregnated into red blood cells featuring bright fluorescence, strong photostability, and lengthened blood residency. *Nano Res*. **2018**, *11*, 2285–2294.

[45] Gu, H. W.; Ho, P. L.; Tsang, K. W. T.; Wang, L.; Xu, B. Using biofunctional magnetic nanoparticles to capture vancomycin-resistant enterococci and other Gram-positive bacteria at ultralow concentration. *J*. *Am*. *Chem*. *Soc*. **2003**, *125*, 15702–15703.

[46] White, A. G.; Fu, N.; Leevy, W. M.; Lee, J. J.; Blasco, M. A.; Smith, B. D. Optical imaging of bacterial infection in living mice using deep-red fluorescent squaraine rotaxane probes. *Bioconjugate Chem*. **2010**, *21*, 1297–1304.

[47] Chudasama, B.; Vala, A. K.; Andhariya, N.; Upadhyay, R. V.; Mehta, R. V. Enhanced antibacterial activity of bifunctional Fe_3O_4-Ag core-shell nanostructures. *Nano Res*. **2009**, *2*, 955–965.

[48] Cai, S. F.; Jia, X. H.; Han, Q. S.; Yan, X. Y.; Yang, R.; Wang, C. Porous Pt/Ag nanoparticles with excellent multifunctional enzyme mimic activities and antibacterial effects. *Nano Res*. **2017**, *10*, 2056–2069.

[49] Stouwdam, J. W.; van Veggel, F. C. J. M. Near-infrared emission of redispersible Er^{3+}, Nd^{3+}, and Ho^{3+} doped LaF_3 nanoparticles. *Nano Lett*. **2002**, *2*, 733–737.

[50] Wang, F.; Xue, X. J.; Liu, X. G. Multicolor tuning of (Ln, P)-doped YVO_4 nanoparticles by single-wavelength excitation. *Angew*. *Chem*., *Int*. *Ed*. **2008**, *47*, 906–909.

[51] Rowe, D. J.; Jeong, J. S.; Mkhoyan, K. A.; Kortshagen, U. R. Phosphorus-doped silicon nanocrystals exhibiting mid-infrared localized surface plasmon resonance. *Nano Lett*. **2013**, *13*, 1317–1322.